Article

SOURCE DATA | TRANSPARENT PROCESS | OPEN ACCESS

THE EMBO JOURNAL

Distinct modes of recruitment of the CCR4–NOT complex by *Drosophila* and vertebrate Nanos

Tobias Raisch†, Dipankar Bhandari†, Kevin Sabath, Sigrun Helms, Eugene Valkov, Oliver Weichenrieder** & Elisa Izaurralde*

Abstract

Nanos proteins repress the expression of target mRNAs by recruiting effector complexes through non-conserved N-terminal regions. In vertebrates, Nanos proteins interact with the NOT1 subunit of the CCR4–NOT effector complex through a NOT1 interacting motif (NIM), which is absent in Nanos orthologs from several invertebrate species. Therefore, it has remained unclear whether the Nanos repressive mechanism is conserved and whether it also involves direct interactions with the CCR4–NOT deadenylase complex in invertebrates. Here, we identify an effector domain (NED) that is necessary for the *Drosophila melanogaster* (*Dm*) Nanos to repress mRNA targets. The NED recruits the CCR4–NOT complex through multiple and redundant binding sites, including a central region that interacts with the NOT module, which comprises the C-terminal domains of NOT1–3. The crystal structure of the NED central region bound to the NOT module reveals an unanticipated bipartite binding interface that contacts NOT1 and NOT3 and is distinct from the NIM of vertebrate Nanos. Thus, despite the absence of sequence conservation, the N-terminal regions of Nanos proteins recruit CCR4–NOT to assemble analogous repressive complexes.

Keywords deadenylation; decapping; mRNA decay; translational repression
Subject Categories RNA Biology; Structural Biology
DOI 10.15252/embj.201593634 | Received 5 December 2015 | Revised 29 January 2016 | Accepted 8 February 2016 | Published online 11 March 2016
The EMBO Journal (2016) 35: 974–990

Introduction

Post-transcriptional mRNA regulation plays an essential role in embryonic development. This regulation is mediated by RNA-binding proteins that control the spatial and temporal expression of target mRNAs through the recruitment of effector complexes (Barckmann & Simonelig, 2013). The RNA-binding proteins of the Nanos family are conserved post-transcriptional mRNA regulators that play essential roles in embryonic germline specification, germline stem cell maintenance, and neuronal homeostasis in *Drosophila melanogaster* (*Dm*) and a wide range of other metazoans (Jaruzelska *et al*, 2003; Tsuda *et al*, 2003; Baines, 2005; Lai & King, 2013). The *Dm* Nanos protein is also required for posterior pattern formation in the embryo (Lehmann & Nüsslein-Volhard, 1991).

Three Nanos paralogs (Nanos1–3) exist in vertebrates and various invertebrate species, whereas there is only one family member in *Dm* and other insects (Subramaniam & Seydoux, 1999; Mochizuki *et al*, 2000; Jaruzelska *et al*, 2003; Tsuda *et al*, 2003). This protein family is defined by a highly conserved CCHC-type zinc-finger (ZnF) domain (Curtis *et al*, 1997; Hashimoto *et al*, 2010) and divergent N- and C-terminal unstructured regions of variable lengths (Fig 1A). The ZnF domain mediates binding to RNA and to Pumilio, a conserved Nanos partner that confers mRNA target specificity (Murata & Wharton, 1995; Curtis *et al*, 1997; Wreden *et al*, 1997; Asaoka-Taguchi *et al*, 1999; Sonoda & Wharton, 1999; Jaruzelska *et al*, 2003). The unstructured regions are required for interaction with effector complexes (Verrotti & Wharton, 2000; Ginter-Matuszewska *et al*, 2011), which include the CCR4–NOT deadenylase complex (Kadyrova *et al*, 2007; Suzuki *et al*, 2010, 2012; Joly *et al*, 2013; Bhandari *et al*, 2014).

The CCR4–NOT complex catalyzes the removal of mRNA poly(A) tails and consequently represses translation. In addition, deadenylation by the CCR4–NOT complex is coupled to decapping and 5′-to-3′ exonucleolytic degradation by XRN1 and can therefore lead to full mRNA degradation in some cellular contexts (Temme *et al*, 2014). Furthermore, the CCR4–NOT complex can also repress translation independently of deadenylation (Cooke *et al*, 2010; Chekulaeva *et al*, 2011; Bawankar *et al*, 2013; Zekri *et al*, 2013).

The CCR4–NOT complex consists of several independent modules that dock with NOT1, a central scaffold subunit (Temme *et al*, 2014). NOT1 consists of independently folded α-helical domains that provide binding sites for the individual modules (Fig EV1A). A central domain of NOT1, structurally related to the middle domain of eIF4G (the NOT1 MIF4G domain), provides a binding site for the catalytic module, which comprises two deadenylases, namely CAF1 (or its paralog POP2) and CCR4a (or its paralog CCR4b).

The C-terminal region of NOT1 contains the NOT1 superfamily homology domain (SHD; Fig EV1A) and assembles with

Department of Biochemistry, Max Planck Institute for Developmental Biology, Tübingen, Germany
*Corresponding author. Tel: +49 7071 6011350; E-mail: elisa.izaurralde@tuebingen.mpg.de
**Corresponding author. Tel: +49 7071 6011358; E-mail: oliver.weichenrieder@tuebingen.mpg.de
†These authors contributed equally to this work

NOT2–NOT3 heterodimers to form the NOT module (Bhaskar *et al*, 2013; Boland *et al*, 2013). The NOT module provides binding sites for RNA-binding proteins, such as vertebrate Nanos and *Dm* Bicaudal-C, which recruit the CCR4–NOT complex to their mRNA targets (Chicoine *et al*, 2007; Suzuki *et al*, 2012; Bhandari *et al*, 2014).

The three vertebrate Nanos paralogs contain a 17-amino acid NOT1-interacting motif (NIM) that binds directly to the NOT1 SHD domain (Suzuki *et al*, 2012; Bhandari *et al*, 2014). Although the NIM is conserved in vertebrate Nanos, Nanos proteins of insects and worms do not have a detectable NIM (Lai *et al*, 2011; Suzuki *et al*, 2012; Bhandari *et al*, 2014). Nevertheless, *Dm* Nanos has been reported to interact with NOT4 through its unstructured N-terminus (Kadyrova *et al*, 2007). However, because NOT4 is not stably associated with the CCR4–NOT complex in metazoans (Lau *et al*, 2009; Temme *et al*, 2010), it has remained unclear whether *Dm* Nanos recruits the CCR4–NOT complex to mRNA targets directly or rather relies on its interaction with additional partners, such as Pumilio (PUM) and Brain tumor (BRAT), to exert its repressive function (Wreden *et al*, 1997; Sonoda & Wharton, 1999, 2001).

In this study, we show that although *Dm* Nanos does not contain a NIM, it interacts directly with the CCR4–NOT complex using an extended region that we termed the Nanos effector domain (NED). The NED overlaps with a region previously shown to contribute to Nanos function in *Dm* embryos (Curtis *et al*, 1997; Arrizabalaga & Lehmann, 1999). The crystal structure of a central region of the NED (termed the NOT module binding region, NBR) bound to the NOT module revealed a bipartite interface that contacts both the NOT1 SHD and the NOT3 NOT-box domains. The binding site for the *Dm* NBR on NOT1 does not overlap with the vertebrate NIM-binding site. These results indicate that Nanos proteins have maintained the ability to interact with the CCR4–NOT complex using divergent motifs in disordered protein regions.

Results

Identification of the *Dm* Nanos effector domain (NED)

To investigate whether *Dm* Nanos possesses intrinsic mRNA repressive activity, we used a λN-based tethering assay in *Dm* S2 cells (Behm-Ansmant *et al*, 2006). This assay enabled the study of Nanos function independently of RNA-binding activity. Tethered *Dm* Nanos caused fourfold repression of a firefly luciferase (F-Luc) reporter containing five binding sites (Box B hairpins) for the λN-tag that were inserted in the 3′ UTR (Fig 1B and C). The reduction in F-Luc activity was predominantly explained by a corresponding decrease in the mRNA abundance (Fig 1B and C) and a shortening of the mRNA half-life (Fig EV1B), indicating that Nanos induces mRNA degradation in S2 cells. Nanos did not affect the expression of an F-Luc reporter lacking the BoxB hairpins (Fig EV1C); thus, Nanos must bind to the mRNA to induce degradation.

To define the sequences in *Dm* Nanos required for the repressive activity, we designed a series of deletion mutants. A Nanos protein lacking the ZnF domain retained the activity of the full-length protein in the tethering assay, whereas the isolated ZnF domain was inactive (Fig 1A–C), as shown previously for vertebrate Nanos (Lai *et al*, 2011; Bhandari *et al*, 2014). Further analyses indicated that a region comprising residues 50–236 retained full repressive activity (Fig 1B and C) and was therefore termed the Nanos effector domain (NED). Conversely, deletion of residues 50–236 (ΔNED) abolished the ability of Nanos to repress the expression of the F-Luc-5BoxB reporter (Fig 1B and C). All protein fragments tested were expressed at comparable levels (Fig 1D), and none of them affected the expression of an F-Luc reporter lacking the BoxB hairpins (Fig EV1C).

The results of the tethering assay were confirmed using a reporter containing the F-Luc ORF fused to the 3′ UTR of the *hunchback* (*hb*) mRNA, a known Nanos target (Wang & Lehmann, 1991; Wreden *et al*, 1997; Sonoda & Wharton, 1999). Nanos degraded this mRNA (Fig 1E–G) but did not significantly affect the expression of an F-Luc reporter containing the *oskar* 3′ UTR (Fig EV1D). Thus, Nanos causes mRNA degradation in S2 cells irrespective of whether it is artificially tethered or binds directly to an mRNA.

Importantly, deletion of the NED strongly impaired the ability of Nanos to repress the F-Luc-*hb* reporter (Fig 1E and F). However, the isolated NED did not repress the expression of this reporter (Fig 1E and F), most likely because it lacks RNA binding capacity. These results indicate that the Nanos NED confers repressive activity but requires the ZnF domain to bind to natural mRNA targets, as reported previously (Curtis *et al*, 1997; Hashimoto *et al*, 2010).

Figure 1. *Dm* Nanos represses translation and promotes mRNA degradation.

A Nanos comprises a highly conserved zinc-finger RNA binding domain (ZnF) and non-conserved N-terminal and C-terminal extensions (gray). NIM, NOT1-interacting motif; NED, Nanos effector domain; NBR, NOT module binding region; N1BM and N3BM, NOT1 and NOT3 binding motifs, respectively. Numbers above the bars indicate residues at domain/motif boundaries.

B Tethering assay using the F-Luc-5BoxB reporter and the indicated λN-HA-tagged proteins in S2 cells. A plasmid expressing R-Luc served as a transfection control. The F-Luc activity (black bars) and mRNA levels (green bars) were normalized to those of the R-Luc transfection control and set to 100 in the presence of the λN-HA-GST. The panel shows mean values ± standard deviations from three independent experiments.

C Northern blot of representative RNA samples corresponding to the experiment shown in (B).

D Western blot analysis of the expression of the λN-HA-tagged proteins used in the experiments shown in (B) and (C). GFP served as a transfection control.

E GFP-tagged Nanos fragments were tested for their ability to repress an F-Luc reporter containing the *hb* 3′ UTR. A plasmid expressing GFP served as a negative control. F-Luc activity (black bars) and mRNA levels (green bars) were normalized to those of an R-Luc transfection control and analyzed as described in (B). The panel shows mean values ± standard deviations from three independent experiments.

F Northern blot of representative RNA samples corresponding to the experiment shown in (E).

G Western blot showing the expression of the GFP-tagged proteins used in (E) and (F). R-Luc-V5 served as a transfection control.

H Tethering assay using the F-Luc-5BoxB-A_{95}-C_7-Hhr reporter and the indicated λN-HA-tagged proteins in S2 cells. F-Luc activity (black bars) and mRNA levels (green bars) were analyzed as described in (B). The panel shows mean values ± standard deviations from three independent experiments.

I Northern blot of representative RNA samples corresponding to the experiment shown in (H).

Source data are available online for this figure.

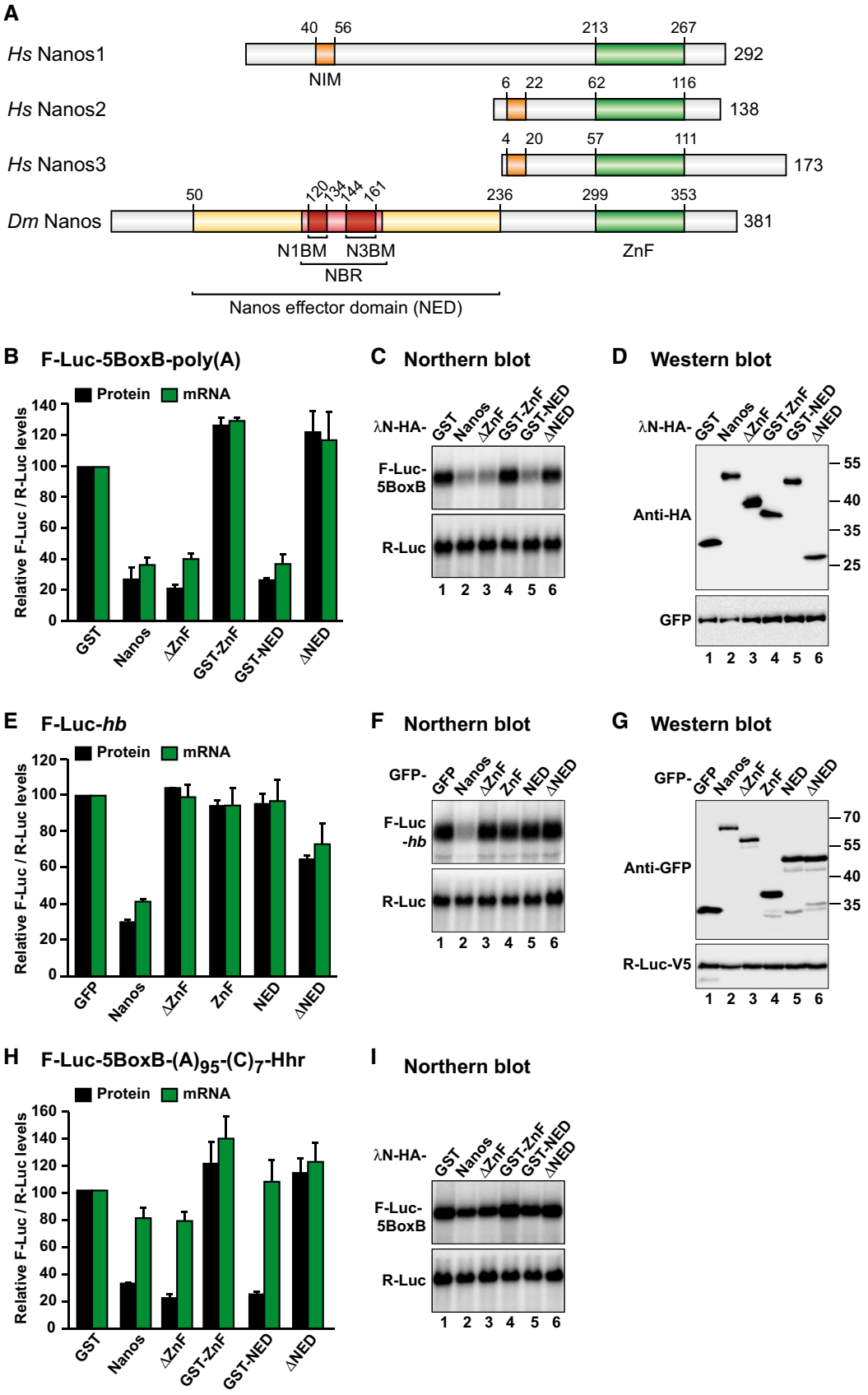

Figure 1.

Nanos mediates translational repression in the absence of mRNA deadenylation

In addition to promoting mRNA target degradation, vertebrate Nanos proteins can repress translation in a deadenylation-independent manner (Lai *et al*, 2011; Bhandari *et al*, 2014). Similarly, *Dm* Nanos promotes deadenylation and represses translation in the absence of mRNA degradation during oogenesis and early embryogenesis (Wharton & Struhl, 1991; Wreden *et al*, 1997; Chagnovich & Lehmann, 2001; Kadyrova *et al*, 2007). Therefore, we investigated whether *Dm* Nanos can repress translation in the absence of mRNA deadenylation in S2 cells. We used an mRNA with a 3′-end generated by a self-cleaving hammerhead ribozyme (HhR). This reporter is neither polyadenylated nor deadenylated (Zekri *et al*, 2013). Additionally, the reporter contains a DNA-encoded poly(A) stretch of 95 nucleotides and a 3′ poly(C) stretch of seven nucleotides upstream of the ribozyme cleavage site (F-Luc-5BoxB-$A_{95}C_7$-HhR). This reporter is efficiently translated in S2 cells (Zekri *et al*, 2013). Tethered Nanos caused a threefold reduction in F-Luc activity but only a 1.2-fold reduction in mRNA levels, indicating that Nanos represses the expression of this reporter primarily at the translational level (Fig 1H and I). Furthermore, a Nanos protein lacking the NED had no repressive activity. Conversely, the NED was sufficient to repress translation of this reporter in the absence of mRNA degradation (Fig 1H and I). Thus, the NED is a major determinant for the repression mediated by *Dm* Nanos irrespective of whether the repression is caused by mRNA deadenylation and decay or by translational repression in the absence of deadenylation.

Nanos has intrinsic repressive activity independent of PUM and BRAT

Nanos functions together with PUM and BRAT to repress *hb* mRNA in *Dm* embryos (Sonoda & Wharton, 1999, 2001). The sequence in the *hb* 3′ UTR that binds PUM, BRAT, and Nanos consists of a duplicated Nanos response element (NRE). Each NRE is composed of one BoxA and one BoxB motif (Fig 2A; Wharton & Struhl, 1991; Murata & Wharton, 1995; Zamore *et al*, 1997; Wreden *et al*, 1997; Wharton *et al*, 1998; Sonoda & Wharton, 1999, 2001; Gupta *et al*, 2009; Loedige *et al*, 2014). BRAT binds to the BoxA motif of the NRE. PUM binds with high affinity to the

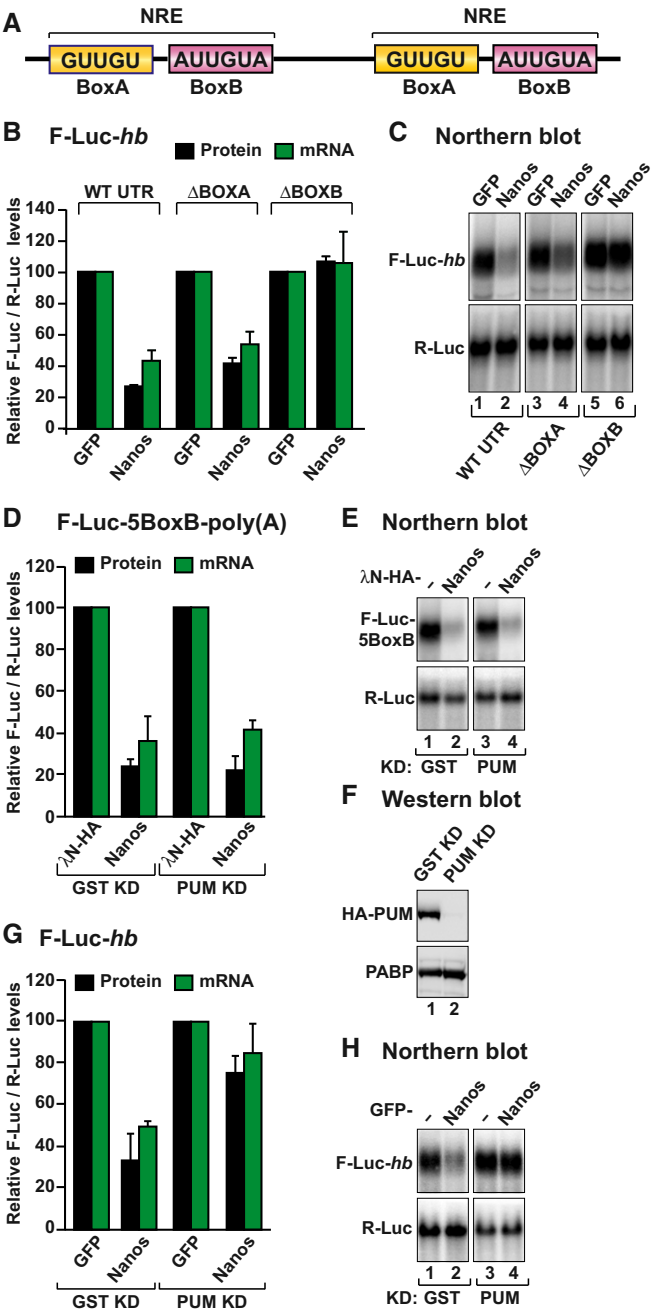

Figure 2. *Dm* Nanos exhibits intrinsic repressive activity.

A Schematic representation of the Nanos response element in the 3′ UTR of *hb* mRNA.

B The activity of GFP-tagged *Dm* Nanos was tested in S2 cells expressing an F-Luc reporter containing the *hb* 3′ UTR (either wild type or mutants lacking the BoxA or BoxB sequences). A plasmid expressing GFP served as a negative control. F-Luc activity (black bars) and mRNA levels (green bars) were analyzed as described in Fig 1B. The panel shows mean values ± standard deviations from three independent experiments.

C Northern blot of representative RNA samples corresponding to the experiment shown in (B).

D Tethering assay using *Dm* Nanos and the F-Luc-5BoxB reporter in S2 cells depleted of PUM or control cells treated with a dsRNA targeting bacterial GST. A plasmid expressing R-Luc mRNA served as a transfection control. The F-Luc activity (black bars) and mRNA levels (green bars) were normalized to those of the R-Luc transfection control and analyzed as described in Fig 1B. The panel shows mean values ± standard deviations from three independent experiments.

E Northern blot of representative RNA samples corresponding to the experiment shown in (D).

F Western blot analysis of S2 cells depleted of PUM and expressing HA-PUM. Endogenous PABP served as a loading control.

G The ability of Nanos to repress the F-Luc-*hb* reporter was tested in S2 cells depleted of PUM as described in (D). The panel shows mean values ± standard deviations from three independent experiments.

H Northern blot of representative RNA samples corresponding to the experiment shown in (G).

Source data are available online for this figure.

BoxB motif but also exhibits low affinity for the BoxA motif (Zamore *et al*, 1997; Wang *et al*, 2002; Gupta *et al*, 2009; Loedige *et al*, 2014, 2015).

To investigate whether Nanos requires BRAT or PUM to repress *hb* mRNA, we tested the effect of deleting the BoxA or BoxB motifs individually from the F-Luc-*hb* reporter. As shown in Fig 1E, transfected Nanos repressed and degraded the F-Luc-*hb* reporter in S2 cells (Fig 2B and C). These cells express both BRAT and PUM but not endogenous Nanos (Miles *et al*, 2012; Weidmann & Goldstrohm, 2012; Loedige *et al*, 2014). The deletion of the BoxA motif did not change the ability of Nanos to repress the reporter. By contrast, deletion of the BoxB sequences abrogated the ability of Nanos to degrade the reporter (Fig 2B), indicating that Nanos cooperates with endogenous PUM to repress the F-Luc-*hb* reporter, as expected (Murata & Wharton, 1995; Wreden *et al*, 1997; Sonoda & Wharton, 1999).

To determine whether Nanos activity in tethering assays was also dependent on its interaction with PUM, we performed the tethering assay in PUM-depleted cells. PUM depletion did not affect Nanos activity in tethering assays (Fig 2D–F) but partially suppressed its ability to repress the F-Luc-*hb* reporter (Fig 2G and H).

In summary, Nanos requires the ZnF domain, PUM, and the BoxB motif to bind to the *hb* 3′ UTR and the NED to repress this mRNA. The requirement for the ZnF domain and PUM is bypassed when Nanos is directly tethered to the mRNA, indicating that *Dm* Nanos possesses intrinsic repressive activity, which is provided by the NED.

Nanos triggers deadenylation-dependent decapping

The vertebrate Nanos proteins trigger deadenylation of mRNA targets by interacting with the CCR4–NOT complex (Suzuki *et al*, 2010, 2012; Bhandari *et al*, 2014). Deadenylation by CCR4–NOT is typically coupled to decapping and 5′-to-3′ exonucleolytic degradation by XRN1 (Temme *et al*, 2014). We therefore investigated whether *Dm* Nanos degrades bound mRNAs by promoting deadenylation-dependent decapping.

If deadenylation precedes decapping and 5′-to-3′ mRNA degradation, then deadenylated mRNA decay intermediates are expected to accumulate in cells in which decapping is inhibited. To inhibit decapping, we overexpressed a catalytically inactive mutant of the decapping enzyme (DCP2*, E361Q) in cells depleted of endogenous DCP2 (Fig 3A and B). In these cells, degradation of the F-Luc-5BoxB reporter by *Dm* Nanos was inhibited and the F-Luc-5BoxB mRNA accumulated as a fast-migrating form, corresponding to the deadenylated decay intermediate (A_0; Fig 3B, lane 5). The luciferase activity is not restored despite restoration of mRNA levels (Fig EV1E), most likely because deadenylated transcripts are translated less efficiently. A similar fast-migrating form accumulated when the GW182 protein was tethered (Fig 3B, lane 6). GW182 is known to cause deadenylation-dependent decapping and thus served as a positive control (Behm-Ansmant *et al*, 2006). The DCP2 mutant was expressed at comparable levels in each condition (Fig EV1F).

To further investigate the dependence on the CCR4–NOT complex for Nanos-mediated mRNA degradation, we depleted NOT3 in S2 cells. NOT3 depletion results in co-depletion of NOT1 and NOT2 (Fig 3C; Temme *et al*, 2010; Boland *et al*, 2013). The ability of Nanos to elicit the degradation of F-Luc-5BoxB mRNA was partially suppressed in NOT3-depleted cells (Fig 3D). Indeed, the half-life of the F-Luc-5BoxB mRNA was increased fourfold in NOT3-depleted cells expressing Nanos relative to that of control cells (Fig 3D).

The NED mediates binding to decay factors

Given that Nanos promotes deadenylation-dependent decapping, we sought to determine whether it interacts with factors involved in the 5′-to-3′ decay pathway. We expressed Nanos with a GFP tag in S2 cells and tested for interactions with HA-tagged subunits of the CCR4–NOT and PAN2–PAN3 deadenylase complexes as well as with decapping factors. Nanos interacted with NOT1, NOT2, NOT3, PAN2, and PAN3 (Figs 4A–D and EV1G–M). These interactions were observed in the presence of RNase A, suggesting that they are not mediated by RNA. In agreement with the tethering assays, the Nanos NED exhibited the same binding properties as full-length Nanos, whereas a Nanos protein lacking the NED did not interact with the deadenylase subunits (Fig 4A–D).

Nanos also interacted with the decapping enzyme DCP2 and the decapping factor HPat in an RNA independent manner but not with additional decapping factors (Figs 4E and F, and EV2A–F). Importantly, the NED was also necessary and sufficient for the interactions with DCP2 and HPat (Fig 4E and F).

The NED interacts directly with the NOT module of the CCR4–NOT complex

To define more precisely how the CCR4–NOT complex interacts with *Dm* Nanos, we used truncated constructs of NOT1, NOT2, and NOT3 in co-immunoprecipitation assays. Deletion of the NOT1 C-terminal region that includes the SHD domain did not abolish the interaction of Nanos with NOT1 (Fig EV2G, lane 12; Fig EV1A and Appendix Table S1). Conversely, the NOT1 C-terminal region was sufficient for Nanos binding (Fig EV2G, lane 10). These results suggest that NOT1 minimally provides two binding sites for Nanos. Additionally, the C-terminal regions of NOT2 and NOT3 were sufficient for Nanos binding (Fig EV2H and I, and Appendix Table S1). The C-terminal regions of NOT2 and NOT3 heterodimerize and interact with the NOT1 SHD to assemble the NOT module (Boland *et al*, 2013), suggesting that Nanos binds to the NOT module. Thus, *Dm* Nanos contains two or more regions that contact the CCR4–NOT complex, of which one binds to the NOT module and one contacts the NOT1 region N-terminal to the SHD.

To determine whether the interaction of Nanos with the NOT module was direct, we performed pull-down assays *in vitro* using purified recombinant proteins expressed in *Escherichia coli*. In this case, we used the human NOT module, which, in contrast to the *Dm* NOT module, is readily expressed in bacteria. The NOT module is highly conserved between the two species with 68, 55, and 72% identity for the NOT1 SHD and the NOT2 and NOT3 C-terminal regions, respectively (Appendix Figs S1 and S2A and B).

The Nanos NED fused N-terminally to glutathione S-transferase (GST) pulled down the preassembled NOT module containing the NOT1 SHD together with the NOT2 and NOT3 C-terminal regions (Fig 5A, lane 12), indicating that the interaction is direct.

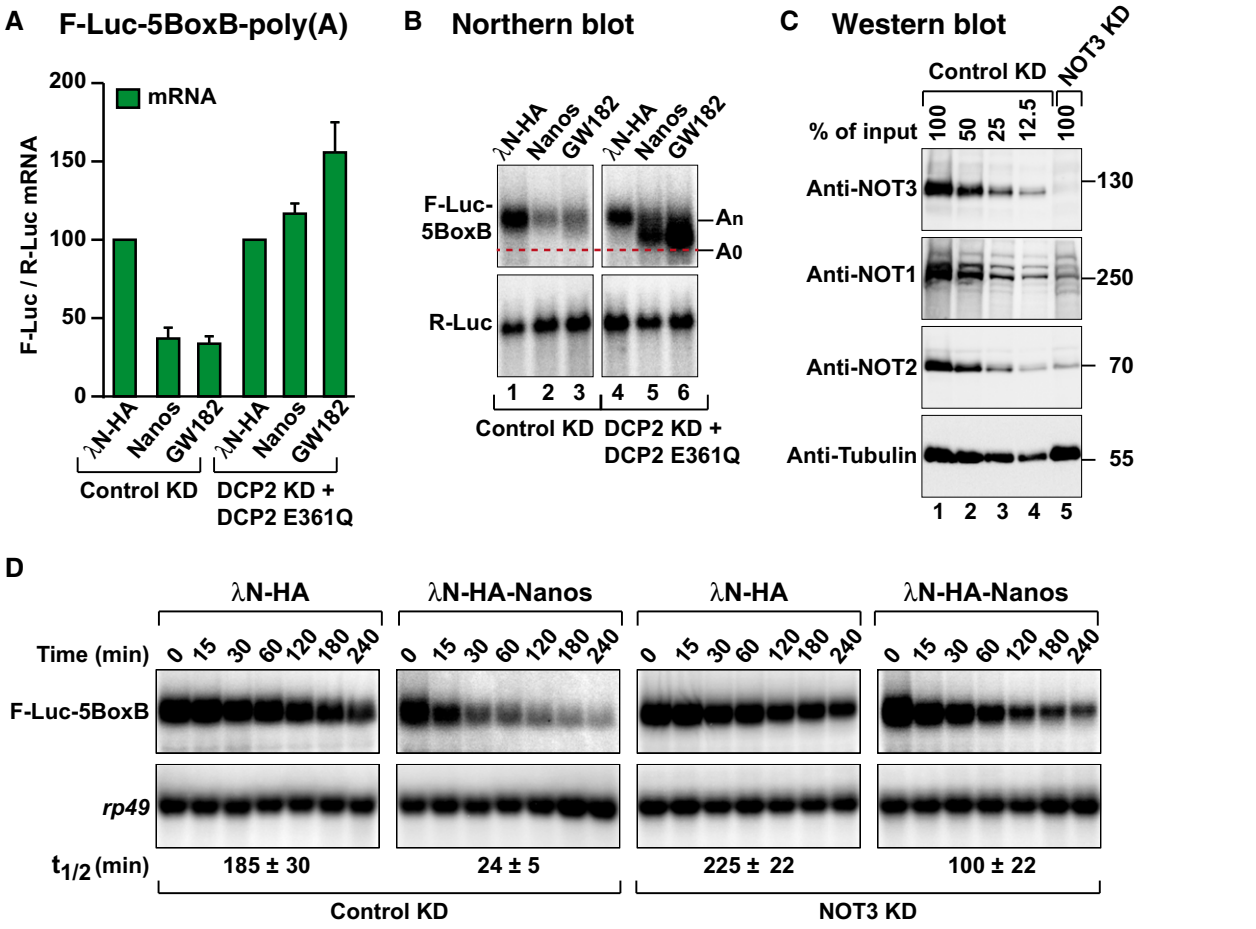

Figure 3. *Dm* Nanos induces deadenylation-dependent decapping.

A Nanos tethering assay using the F-Luc-5BoxB reporter in control cells (treated with GST dsRNA) or in cells depleted of the decapping enzyme DCP2 (DCP2 KD) and expressing a catalytically inactive DCP2 mutant (E361Q). F-Luc activity and mRNA levels were normalized to those of an R-Luc transfection control and analyzed as described in Fig 1B. Normalized F-Luc activities are shown in Fig EV1E. The panel shows mean values ± standard deviations from three independent experiments.

B Northern blot of representative RNA samples corresponding to the experiment shown in (A). The positions of the polyadenylated (A_n) and deadenylated (A_0) F-Luc-5BoxB mRNA are indicated on the right.

C Western blot analysis of S2 cells depleted of NOT3. Dilutions of control cell lysates were loaded in lanes 1–4 to estimate the efficacy of the depletion. α-Tubulin served as a loading control. KD: knockdown. Endogenous NOT1 and NOT2 are co-depleted with NOT3 as described previously (Boland *et al*, 2013).

D Northern blot analysis showing the decay of the F-Luc-5BoxB mRNA in control cells (treated with GST dsRNA) or in cells depleted of NOT3 expressing the indicated proteins. The mRNA half-lives ($t_{1/2}$) ± standard deviations calculated from the decay curves of three independent experiments are indicated below the panels.

Source data are available online for this figure.

The NED consists of several motifs that act redundantly to recruit the CCR4–NOT complex

To define the sequence requirements for binding of the *Dm* Nanos NED to the NOT module, we analyzed the alignment of NED sequences from various *Drosophila* species, which revealed three blocks of conserved residues (50–112, 116–163, and 207–236; Fig EV3A). Remarkably, each of these protein regions in isolation exhibited repressive activity in tethering assays, indicating functional redundancy (Fig EV3B–D). However, only the fragment comprising residues 116–163 was sufficient for binding to the purified NOT module complex *in vitro* (Fig 5A, lane 16, NBR), whereas deletion of residues 116–163 in the context of the NED abolished binding to the NOT module (Fig 5A, lane 14, ΔNBR). Thus, residues 116–163 within the NED represent a NOT module binding region (NBR).

The vertebrate Nanos NIM interacts directly with the NOT1 C-terminal SHD domain and does not contact NOT2 or NOT3 (Bhandari *et al*, 2014). We therefore determined whether the *Dm* NBR interacted with the purified NOT1 SHD. However, the NBR interacted exclusively with the assembled NOT module but not with the isolated NOT1 SHD or the NOT2–NOT3 dimer (Fig 5B, lanes 14–16), indicating that the *Dm* NBR requires the entire NOT module for binding. Thus, the *Dm* NBR and the vertebrate NIM interact with the NOT module using different binding modes. Accordingly, the vertebrate Nanos3 NIM peptide (when added in excess to the NBR) did not compete with the NBR for binding to the NOT module; instead, both peptides bound simultaneously (Fig EV3E, lane 8).

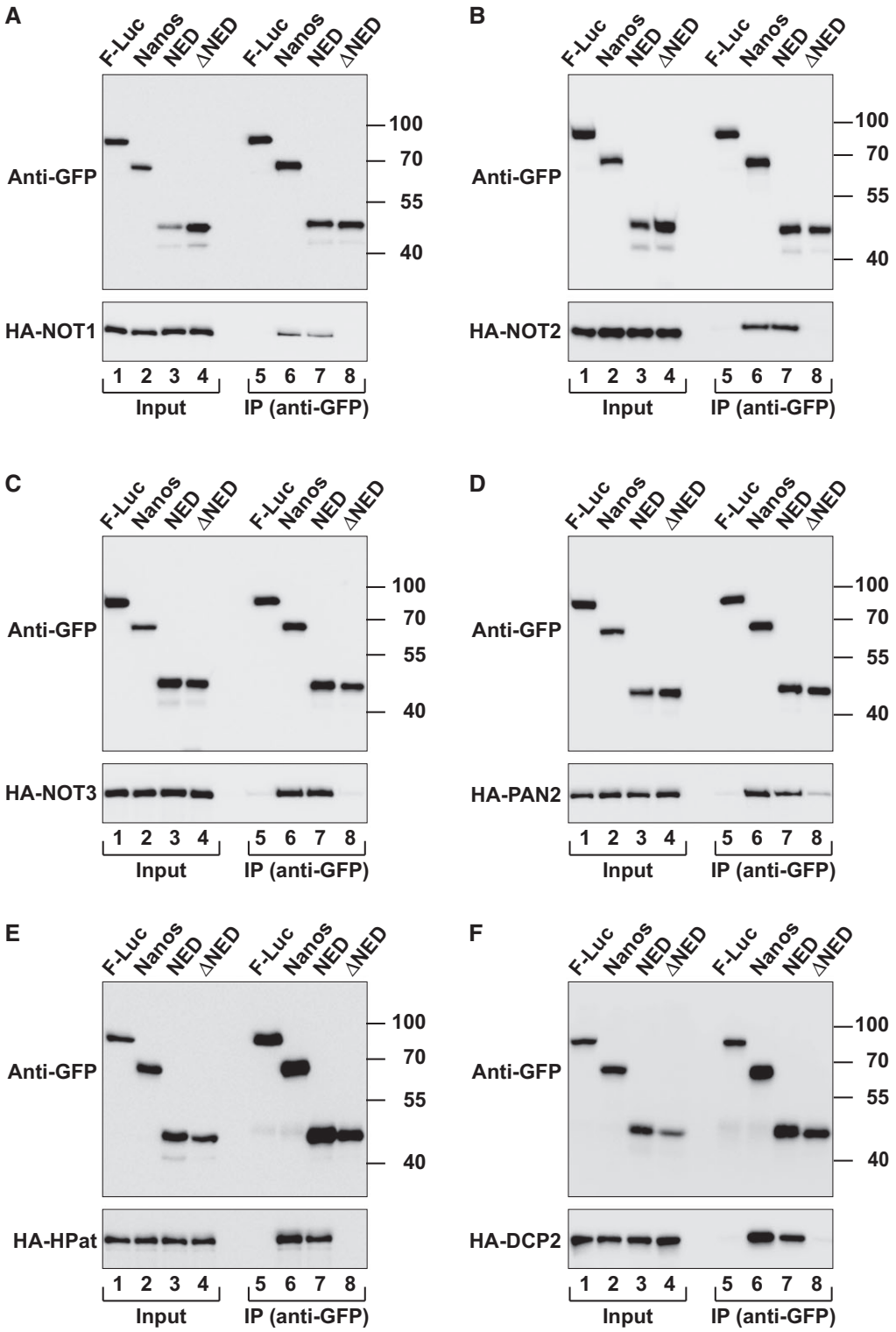

Figure 4. The Nanos NED interacts with subunits of the deadenylase and decapping complexes.

A–F Western blots showing the interaction of GFP-tagged *Dm* Nanos (either full length, NED, or ΔNED) and the indicated HA-tagged proteins. The co-immunoprecipitations were performed using a polyclonal anti-GFP antibody. GFP-tagged firefly luciferase (F-Luc) served as a negative control. Inputs and immunoprecipitates were analyzed using anti-GFP and anti-HA antibodies. For the GFP-tagged proteins, 3% of the inputs and 10% of the immunoprecipitates were loaded, whereas for the HA-tagged proteins, 1% of the input and 30% of the immunoprecipitates were analyzed. In all panels, cell lysates were treated with RNase A prior to immunoprecipitation.

Source data are available online for this figure.

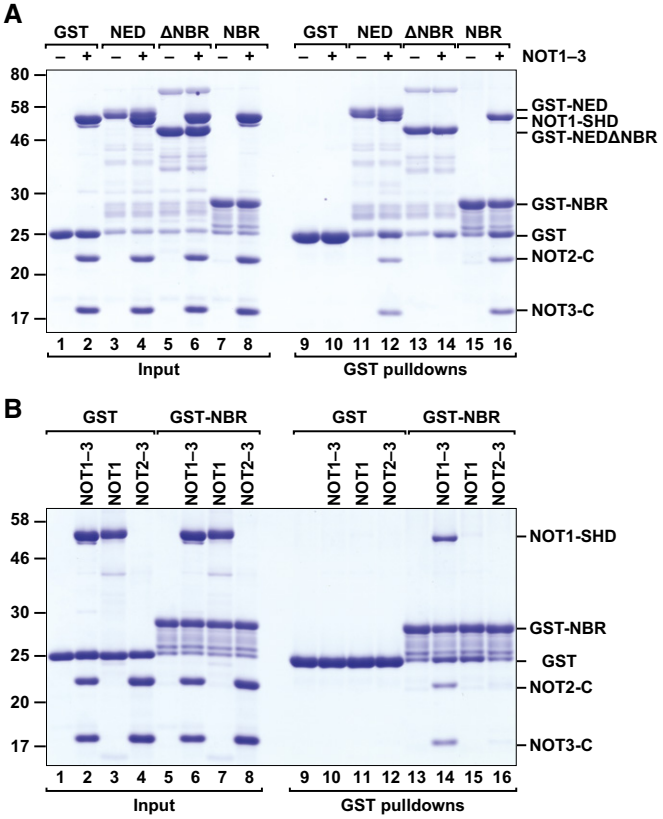

Figure 5. The central region of the Nanos NED interacts directly with the NOT module.

A GST pull-down assay showing the interaction of the GST-tagged *Dm* Nanos NED (wild type or lacking the NBR) and GST-NBR with the recombinant *Hs* NOT module (NOT1–3; containing the NOT1 SHD and the NOT2 and NOT3 C-terminal fragments).

B GST pull-down assay showing the interaction of the GST-tagged *Dm* Nanos NBR with the assembled NOT module (NOT1–3), the isolated NOT1 SHD (NOT1), or the NOT2–NOT3 dimers (NOT2–3).

Source data are available online for this figure.

Crystal structure of the *Dm* Nanos NBR bound to the NOT module

To explain the complexity of the interaction of the *Dm* NBR with the NOT module, we sought to obtain structural information. However, the failure to express soluble *Dm* NOT1 SHD in *E. coli* precluded the reconstitution of the *Dm* NOT module. Therefore, we turned to the human NOT module. On the basis of the available structure, we introduced mutations into the NOT1 SHD to improve crystallization. A triple substitution in the most C-terminal loop of the NOT1 SHD domain (L19; Appendix Table S1 and Appendix Fig S1) resulted in highly reproducible crystals of the NOT module from which we obtained a structure at an improved resolution of 2.9 Å and in a new crystal packing environment with two copies of the complex per asymmetric unit (Fig EV4A and Table 1).

Furthermore, we also obtained the structure of the NOT module mutant in complex with the *Dm* Nanos NBR peptide at 3.1 Å resolution, which exhibited highly similar crystal packing and unit cell parameters closely related to the apo structure (Figs 6A and B, and EV4B and Table 1). The two copies of the complex in the asymmetric unit are structurally highly similar (Fig EV4C and D; RMSD 0.22 Å over 817 C_αs), and the *Dm* Nanos NBR peptide does not induce any major conformational changes in the NOT module (Fig EV4B; RMSD of 0.37 Å over 706 C_αs for the NOT module mutants in the bound and apo states).

The most obvious difference to the previously reported structure of the human NOT module (Boland *et al*, 2013) is the formation of an additional α-helix (α22') as part of the mutated loop L19 and the reorientation of the NOT1 C-terminal helix α23 in both copies of the asymmetric unit (Fig EV4A and E). The rearrangement is probably due to the loss of crystal contacts by the mutated loop L19 sequence that can also explain the improved crystallization of the NOT module mutant compared with that of the wild type. Because helix α23 is now in a similar conformation as that in the complex of the NOT1 SHD domain with the *Hs* Nanos1 NIM peptide (Fig EV4F; Bhandari *et al*, 2014), we propose that this is the preferred conformation of helix α23.

Most strikingly, the *Dm* Nanos NBR peptide binds in a completely different location on the surface of the NOT module compared to the *Hs* Nanos1 NIM peptide (Fig 6C). Moreover, the *Dm* Nanos NBR peptide shows a very distinct bipartite binding mode, and it extends over the surfaces of both NOT1 and NOT3. The *Dm* Nanos NBR peptide folds into two α-helices connected by a disordered linker region with lower sequence conservation (Figs 6A and B, and EV3A). The first α-helix binds to the NOT1 SHD and represents the NOT1-binding motif (N1BM, residues 120–134), whereas the second α-helix is part of the NOT3-binding motif (N3BM, residues 144–161) and binds to the NOT3–NOT-box domain.

Interactions of the N1BM and the N3BM

As previously described, the NOT1 SHD consists of two perpendicular stacks of HEAT-like repeats (Bhaskar *et al*, 2013; Boland *et al*, 2013). The NOT2 and NOT3 NOT-box domains each adopt an SH3-like fold comprising a five-stranded half-open β-barrel as well as two and three α-helices, respectively, which mediate heterodimerization. Furthermore, NOT2 and NOT3 have N-terminal extensions that serve to embrace each other's NOT-box domains and to tether the NOT2–NOT3 heterodimer to the surface of the NOT1 SHD (Fig 6A and B).

The N1BM folds into a three-turn amphipathic α-helix that docks into a groove on the surface of the NOT1 SHD (Figs 6D–F and EV4G). This groove forms between the termini of α-helices 3 and 4 (HEAT repeat 2), and the flanking HEAT repeats 1 and 3 of the SHD. The hydrophobic surface of the N1BM α-helix faces the groove with residues I123, A124, L127, and F130. These residues are matched by NOT1 SHD residues F1876, V1880, L1889, I1895, L1946, H1949, and L1962, leading to a predominantly hydrophobic interaction (Figs 6D–F, EV3A, EV4G, and Appendix Fig S1).

The N3BM also folds into an amphipathic helix. This helix docks onto the open side of the β-barrel in the NOT3–NOT-box domain, and it is additionally extended by a short β-strand that augments the highly curved β-sheet of the barrel (Figs 6G–I and EV4H and I). Again, the interaction is primarily hydrophobic with residues M145, V148, M149, and, in particular, F152 from the N3BM facing residues Y702, M703, M704, F706, Y726, Y729, K737, and F740 on the NOT3–NOT-box (Figs 6G–I, EV3A, EV4H and I, and Appendix Fig S2B). Notably, the NOT3 residues Y702, F706, Y726, and F740 surround

Table 1. Data collection and refinement statistics.

	NOT123–Nanos	NOT123–Nanos SeMet	NOT123 apo
Space group	P 2_1	P 2_1	P 2_1
Unit cell			
dimensions *a*, *b*, *c* (Å)	76.0, 135.7, 105.0	77.1, 135.8, 105.8	76.0, 135.3, 101.3
angles α, β, γ (°)	90, 108, 90	90, 108, 90	90, 108, 90
Data collection[a]			
Wavelength (Å)	1.00005	0.97866	0.99982
Resolution range (Å)	50–3.1 (3.17–3.10)	50–3.9 (4.00–3.90)	50–2.9 (2.98–2.90)
R_{sym} (%)	7.5 (74.1)	20.7 (81.3)	7.5 (63.3)
Completeness (%)	99.6 (98.2)	99.7 (98.1)	99.4 (99.7)
Mean $I/\sigma(I)$	13.0 (1.7)	8.6 (2.4)	11.9 (2.1)
Unique reflections	36,658 (2,706)	18,985 (1,369)	43,109 (3,191)
Multiplicity	3.45 (3.45)	6.92 (6.78)	3.26 (3.27)
Refinement			
R_{cryst} (%)	16.5		18.1
R_{free} (%)	22.7		22.1
Coordinate error (Å)	0.42		0.35
Number of atoms			
All atoms	14,548		14,109
Protein	14,548		14,109
Water	0		0
Average B factor (Å^2)			
All atoms	99.3		83.9
Ramachandran plot			
Favored regions (%)	95.3		95.8
Disallowed regions (%)	0.3		0.4
RMSD from ideal geometry			
Bond lengths (Å)	0.010		0.010
Bond angles (°)	1.10		1.10

[a]Values in parentheses are for highest resolution shell.

the aromatic ring of F152, and Y702 makes additional hydrogen bonds to E151 and N155 of N3BM (Figs 6I and EV4H). Furthermore, K737 contacts the F152 and G156 carbonyl oxygens and serves as an anchor for the following residues and stabilizes their main-chain interactions with the outer edge of the NOT3 β-sheet (Fig EV4I).

To confirm the sequence assignment of the relatively short N1BM and N3BM in the 3.1 Å electron density, we substituted I123 in the N1BM with methionine and crystallized the complex with a selenomethionine-derivatized *Dm* Nanos mutant peptide. This allowed us to collect anomalous diffraction data using X-ray energies at the selenium K-edge (Table 1) and to calculate an anomalous difference Fourier map (Fig EV5A–D). The map unambiguously identified M123 in the N1BM as well as M145 and M149 in the N3BM, confirming that our initial sequence assignment was correct.

Validation of the binding interfaces

To confirm that the interfaces from the crystal structure are also relevant in solution, we introduced mutations in the Nanos peptide, NOT1 or NOT3, and tested binding of the peptide to the preassembled NOT modules using GST pull-down assays *in vitro*. To validate the N1BM–NOT1 interface, we generated the NOT1 mutants V1880E and H1949D (corresponding to *Dm* NOT1 V2002E and H2067D, respectively). These mutations strongly reduced but did not abolish binding of the GST-NBR fusion to the NOT module (Fig 7A, lanes 17 and 18 vs. 16). Conversely, the mutations in the Nanos N1BM (2xMut, L127D, F130D) strongly reduced binding to the NOT module (Fig 7A, lane 20).

To validate the N3BM–NOT3 interaction, we substituted the central NOT3 residue Y702 with alanine (Y702A). This mutation was sufficient to abolish binding of the NBR to the NOT module (Fig 7B, lane 16 vs. 15). Conversely, the F152E mutation in the *Dm* Nanos N3BM was sufficient to disrupt complex assembly (Fig 7B, lane 20), confirming the central role of this residue in the interaction. Because no residual binding was observed for the Nanos F152E mutant despite the presence of the N1BM, these results indicate that the N1BM is not sufficient for complex formation.

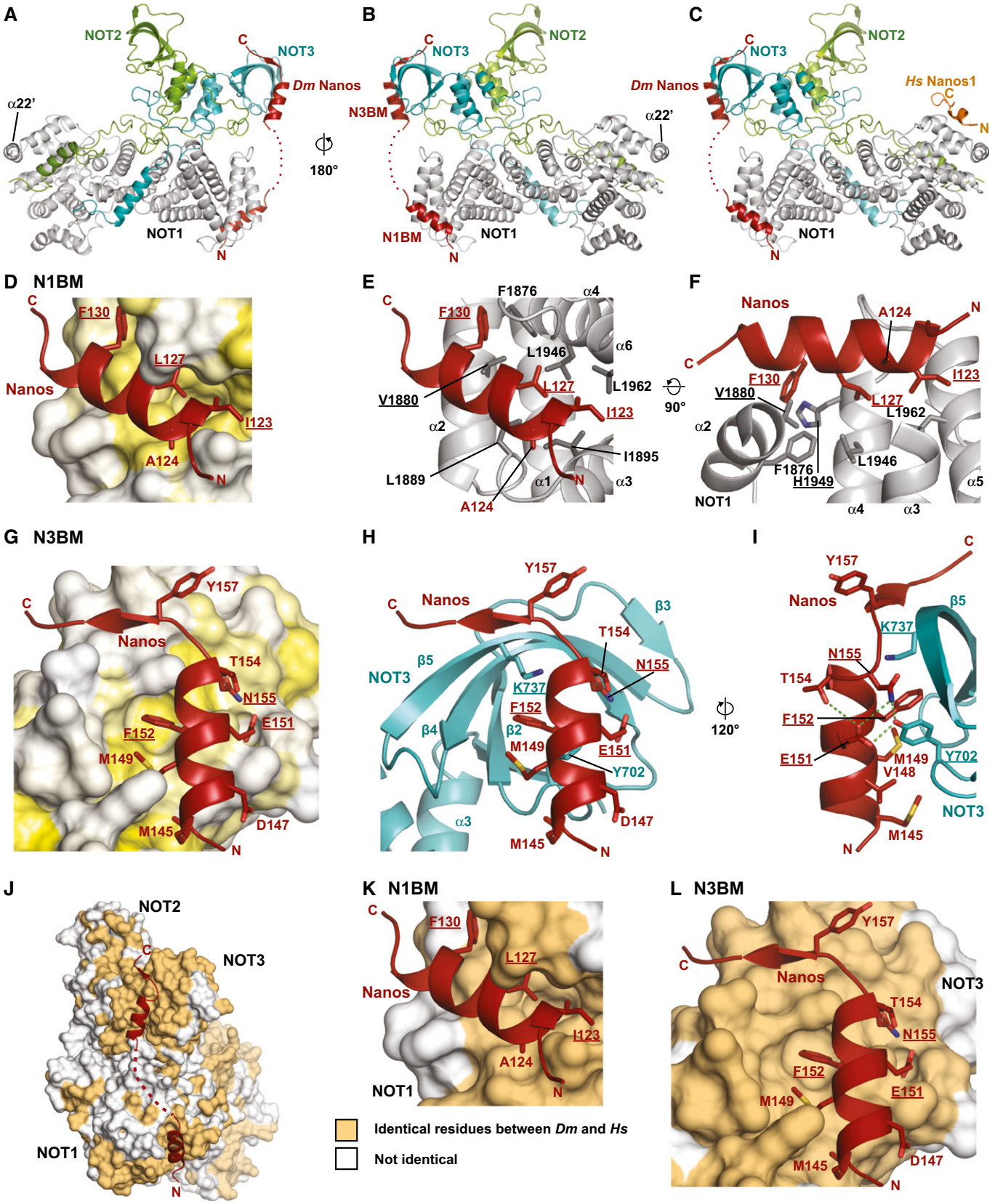

Figure 6.

Figure 6. Structure of the *Dm* Nanos NBR bound to the NOT module.

A, B Cartoon representation of the *Dm* NBR peptide (red) bound to the NOT module in two orientations. The NOT1 SHD is colored in gray. NOT2 and NOT3 are shown in green and cyan, respectively.

C Model including the Nanos1 NIM peptide (from PDB entry 4CQO, Bhandari *et al*, 2014) obtained by superimposing the NOT1 SHD domains.

D Surface representation of the N1BM binding pocket of NOT1 with residues colored in a gradient from white to yellow with increasing hydrophobicity according to Kyte and Doolittle (1982).

E Cartoon representation of the N1BM binding pocket. Selected residues of NOT1 and of the NBR peptide are shown as gray and red sticks, respectively. Residues mutated in this study are underlined.

F Alternative view of the N1BM binding pocket. NOT1 residues 1883–1894 of loop L2 have been omitted for clarity. Residues mutated in this study are underlined.

G Surface representation of the N3BM binding pocket of NOT3 colored as described in (D).

H Cartoon representation of the N3BM binding pocket. Selected residues of NOT3 and of the NBR peptide are shown as cyan and red sticks, respectively. Residues mutated in this study are underlined.

I Alternative view of the N3BM binding pocket including selected hydrogen bonds as dashed green lines. Residues mutated in this study are underlined.

J–L Conservation of the NBR binding sites on the NOT module surface. The NOT module is shown in surface representation. Surface residues that are identical between *Hs* and *Dm* are shown in orange, all other residues are shown in white. The views shown in (K) and (L) are in the same orientation as those shown in (D) and (G), respectively.

The residues in NOT1 and NOT3 interacting with the Nanos peptide are conserved in *Dm* (Fig 6J–L, and Appendix Figs S1 and S2B). Nevertheless, it was important to assess whether *Dm* Nanos binds to the *Dm* NOT module using a similar binding mode. To this end, we used the recombinant GST fusions of *Dm* Nanos NBR mutants described above and tested the interactions with the endogenous *Dm* CCR4–NOT complex in *Dm* S2 cell lysates. Mutations in the N1BM (2xMut) or in the N3BM (F152E or 3xMut (E151A F152A N155A); Appendix Table S1) were sufficient to disrupt the interaction (Fig 7C, lanes 8–10). In agreement with these results, the mutations abolished the activity of the NBR in tethering assays (Fig 7D–F). Notably, the mutations were ineffectual in the context of full-length Nanos (Fig EV5E–H), in agreement with the notion that the NED contains multiple sequences that mediate the recruitment of the CCR4–NOT complex in a redundant manner.

The vertebrate Nanos NIM and the *Dm* NED perform analogous functions

Given that the *Dm* NED and the vertebrate NIM recruit the CCR4–NOT complex, we asked whether the NED could be replaced by the human Nanos NIM and elicit mRNA degradation in *Dm* cells. To test this hypothesis, we generated a chimeric protein containing the human Nanos2 NIM fused to the *Dm* Nanos ZnF domain (NIM–ZnF). This protein effectively repressed and degraded the F-Luc-5BoxB mRNA reporter in the tethering assays (Fig 8A and B). Importantly, the chimeric protein also degraded the F-Luc-*hb* reporter (Fig 8C and D) and interacted with the *Dm* CCR4–NOT complex (Fig 8E). Mutations of conserved aromatic residues in the NIM motif (NIM*: F6A and W9E; Appendix Table S1), which are essential for binding to the human NOT module (Bhandari *et al*, 2014), abolished the interaction of the chimeric protein with the *Dm* CCR4–NOT complex and the ability of the protein to degrade the F-Luc-5BoxB and F-Luc-*hb* mRNAs (Fig 8A–E). These results indicate that the vertebrate NIM interacts with the *Dm* CCR4–NOT complex using an interaction mode similar to that observed for the human complex. Accordingly, the NOT1 residues required for the interaction with the NIM are conserved in *Dm* (Appendix Fig S1; Bhandari *et al*, 2014).

We also tested whether *Dm* Nanos repressed the expression of a reporter in tethering assays in human cells. We observed that both *Dm* Nanos and the NED caused mRNA degradation in tethering assays in human cells and interacted with human NOT3 (Fig 8F–H). Furthermore, when the NIM was replaced by the NBR in human Nanos2, the chimeric protein degraded the mRNA reporter and interacted with the endogenous CCR4–NOT complex in HEK293T cells (Fig EV5I–L).

Discussion

In this study, we showed that *Dm* Nanos recruits the CCR4–NOT complex directly through a Nanos effector domain (NED) that is conserved in the *Drosophila* species (Fig EV3). Similar to the vertebrate Nanos NIM, the *Dm* NED is necessary and sufficient to repress

Figure 7. Validation of the interaction interfaces.

A GST pull-down assay showing the interaction of the GST-*Dm* Nanos NBR [wild type or 2xMut (L127D F130D)] with the recombinant NOT module (NOT1–3) containing the NOT1 SHD (either wild type or V1880E and H1949D). GST served as a negative control. Note that the GST-*Dm* Nanos NBR 2xMut exhibits abnormal electrophoretic migration most likely due to the introduction of two negatively charged residues.

B GST pull-down assay showing the interaction of GST-*Dm* Nanos NBR [wild type, F152E and 3xMut (E151A, F152A, N155A)] with the recombinant NOT module containing wild-type NOT3 or the Y702A mutant. GST served as a negative control.

C GST pull-down assay showing the interaction of GST-tagged *Dm* Nanos NBR (wild type, F152E, 2xMut, and 3xMut) with the *Dm* CCR4–NOT complex in S2 cell lysates. GST served as a negative control.

D Tethering assay using the Nanos NBR mutants and the F-Luc-5BoxB reporter in S2 cells. A plasmid expressing R-Luc mRNA served as a transfection control. The F-Luc activity (black bars) and mRNA levels (green bars) were analyzed as described in Fig 1B. The panel shows mean values ± standard deviations from three independent experiments.

E Northern blot of representative RNA samples corresponding to the experiment shown in (D).

F Western blot showing the expression of the λN-HA-tagged proteins used in the experiments shown in (D) and (E). GFP served as a transfection and loading control.

Source data are available online for this figure.

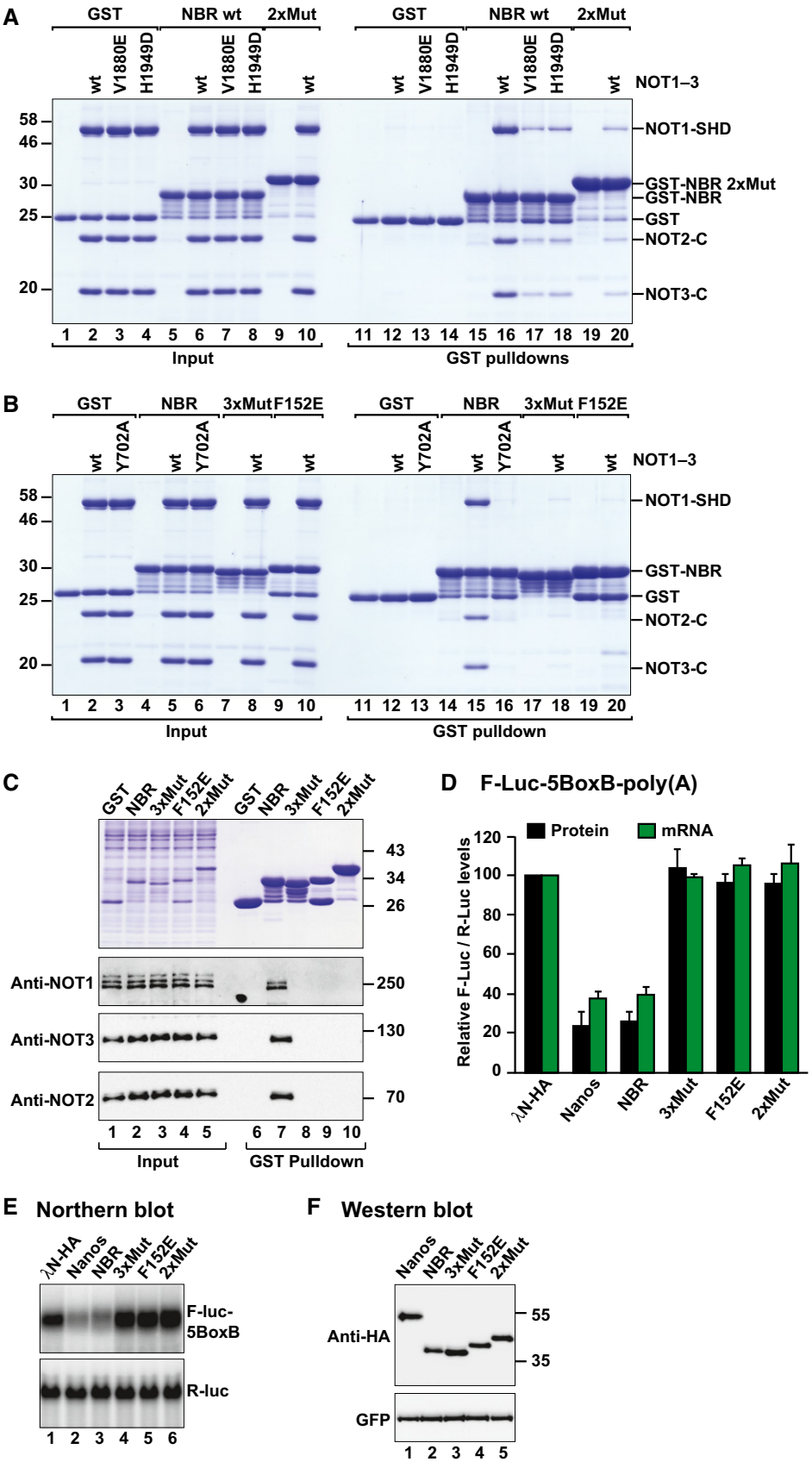

Figure 7.

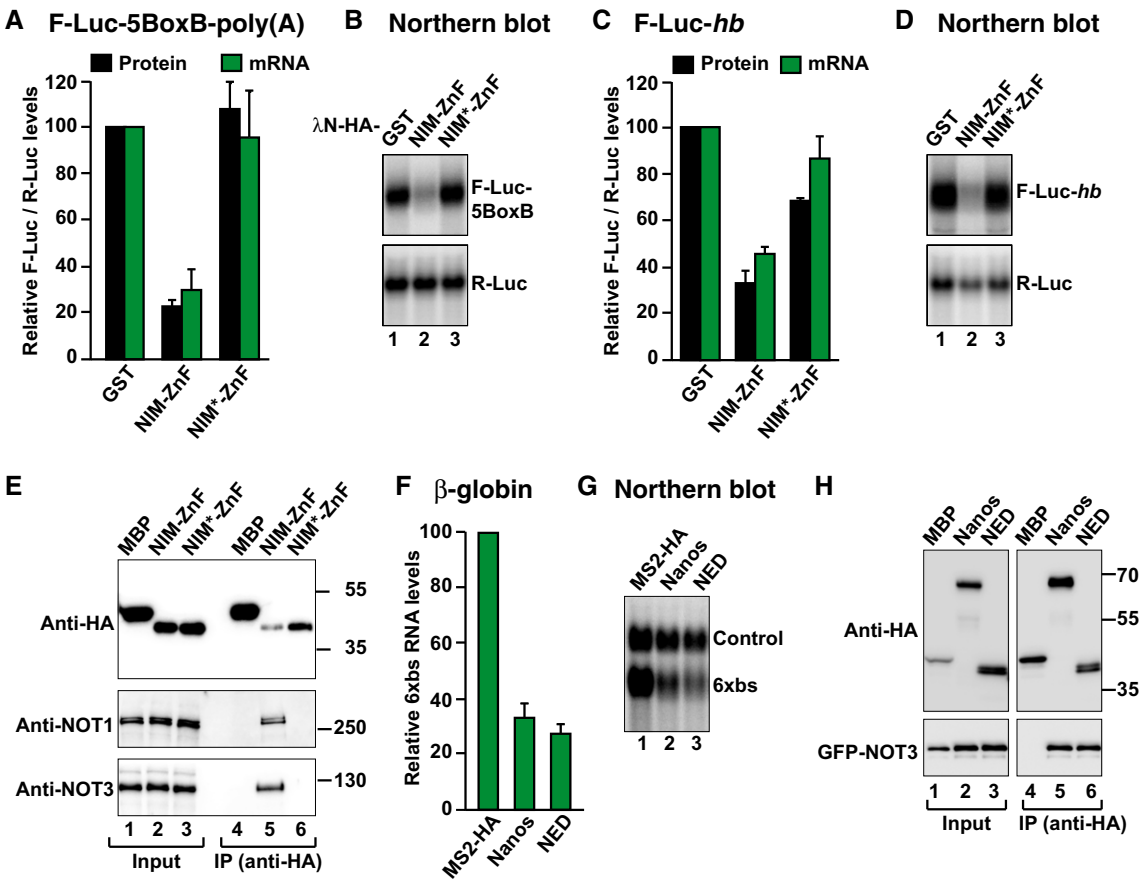

Figure 8. The NED and NIM are functionally equivalent.

A Tethering assay using a chimeric Nanos protein and the F-Luc-5BoxB reporter in S2 cells. The chimeric Nanos protein contains the NIM of human Nanos2 (either wild type (NIM-ZnF) or mutated (NIM*-ZnF)), fused to the *Dm* ZnF domain. A plasmid expressing GST served as a negative control. F-Luc activity and mRNA levels were analyzed as described in Fig 1B. The panel shows mean values ± standard deviations from three independent experiments.

B Northern blot of representative RNA samples corresponding to the experiment shown in (A).

C The activity of GST-HA-tagged Nanos chimeric protein was tested in S2 cells expressing an F-Luc-*hb* reporter. A plasmid expressing GST served as a negative control. F-Luc activity and mRNA levels were analyzed as described in Fig 1B. The panel shows mean values ± standard deviations from three independent experiments.

D Northern blot of representative RNA samples corresponding to the experiment shown in (C).

E Western blot analysis showing the interaction of the HA-tagged Nanos chimeric protein (NIM-ZnF or NIM*-ZnF) with endogenous *Dm* NOT1 and NOT3. HA-MBP served as a negative control.

F Tethering assays in human HEK293T cells, using a β-globin reporter containing 6 binding sites (6xbs) for the MS2 protein and MS2-HA-tagged *Dm* Nanos or NED fragment. A plasmid expressing an mRNA lacking MS2 binding sites (Control) served as a transfection control. The β-globin-6xbs mRNA levels were normalized to those of the control mRNA and set to 100 in the presence of MS2-HA. The panel shows mean values ± standard deviations from three independent experiments.

G Northern blot of representative RNA samples corresponding to the experiment shown in (F).

H Co-immunoprecipitation assay in human HEK293T cells showing the interaction of the HA-tagged *Dm* Nanos and the NED fragment with GFP-tagged NOT3 in human cells. HA-MBP served as a negative control. The inputs (1%) and bound fractions (10% of HA-tagged proteins and 30% of GFP-NOT3) were analyzed by Western blotting.

Source data are available online for this figure.

translation in the absence of mRNA degradation and to promote degradation of bound mRNAs. Thus, the NED and the NIM are the main determinants for the repressive activity of Nanos in *Dm* and vertebrates, respectively. Although the NED and the NIM are functionally analogous, they do not share sequence similarities, demonstrating that the absence of sequence conservation is not an indicator of functional irrelevance, in particular, when disordered, low complexity protein regions are involved. Such regions often mediate their function by interacting with binding partners using short linear motifs (SLiMs). SLiMs can evolve rapidly due to the lack of constraints to maintain a protein fold (Davey *et al*, 2012) and thus enable the evolution of distinct binding modes in orthologous proteins, especially in cases where these proteins are in a competitive scenario or even under positive selection. In this way, these proteins can maintain the ability to interact with the same partners using different binding modes.

The *Dm* NED uses multiple and redundant motifs to recruit the CCR4–NOT complex

The *Dm* NED and the vertebrate NIM use different modes to mediate the recruitment of the CCR4–NOT complex to Nanos mRNA

targets. The NIM is a short 17-residue motif present in the N-terminal disordered region of vertebrate Nanos proteins, which binds to the NOT1 SHD domain (Bhandari *et al*, 2014). In contrast to vertebrates, flies have only a single Nanos protein but with an extended NED. The *Dm* NED is 187 amino acids in length and contains multiple and redundant binding sites for the CCR4–NOT complex. These multiple binding sites may increase the affinity of *Dm* Nanos for the CCR4–NOT complex through avidity effects. Redundancy may also confer a competitive advantage to *Dm* Nanos over other RNA-binding proteins that compete for recruitment of the CCR4–NOT complex.

Interestingly, redundancy to recruit the CCR4–NOT complex is not only observed within the Nanos protein but also in the context of Nanos repressive complexes. Indeed, Nanos cooperates with PUM to bind and repress natural mRNA targets, and PUM also has the ability to recruit the CCR4–NOT complex independently of Nanos (Asaoka-Taguchi *et al*, 1999; Sonoda & Wharton, 1999, 2001; Jaruzelska *et al*, 2003; Goldstrohm *et al*, 2006; Van Etten *et al*, 2012). This may partially obscure the effects of deletion or mutations in the Nanos NED. However, PUM does not act as a general substitute for Nanos because mutations in the Nanos ZnF domain that prevent mRNA binding caused strong developmental defects despite the presence of endogenous PUM (Arrizabalaga & Lehmann, 1999). Thus, PUM probably acts both additively and alternatively with the Nanos NED, resulting in distinct modes of engaging the CCR4–NOT complex. In their various combinations, the different binding modes can thus lead to a highly specific and tunable repression of mRNA targets in a cell context-dependent manner.

RNA-binding proteins recruit CCR4–NOT using a diversity of binding motifs

A large number of RNA-associated proteins have been shown to recruit the CCR4–NOT complex to their mRNA targets to repress translation and/or to promote mRNA degradation. In addition to Nanos, these proteins include the GW182 proteins, which are involved in miRNA-mediated gene silencing in animals, and the *Dm* proteins CUP, Bicaudal-C, Smaug, and PUM (Semotok *et al*, 2005; Goldstrohm *et al*, 2006; Chicoine *et al*, 2007; Igreja & Izaurralde, 2011; Van Etten *et al*, 2012; Chen *et al*, 2014; Mathys *et al*, 2014). Additional examples from vertebrates are Roquin and tristetraprolin (TTP), a protein required for the degradation of mRNAs containing AU-rich elements (ARE-mediated mRNA decay) (Fabian *et al*, 2013; Leppek *et al*, 2013).

For the recruitment of the CCR4–NOT complex, most of these proteins rely on short linear motifs (SLiMs) embedded in peptide regions of predicted disorder. However, a detailed characterization of their interaction with the CCR4–NOT complex on a molecular level is only available for TTP, GW182, and vertebrate and *Dm* Nanos (Fabian *et al*, 2013; Bhandari *et al*, 2014; Chen *et al*, 2014; Mathys *et al*, 2014; this study). For TTP and vertebrate and *Dm* Nanos, the motifs adopt α-helical conformations that possibly form only upon binding. Specificity results from aromatic and hydrophobic side chains that insert primarily into pockets on the surface of the NOT1 domains that consist of HEAT-like repeats (Fabian *et al*, 2013; Bhandari *et al*, 2014; this study). By contrast, GW182 peptides likely bind to the CCR4–NOT complex in an extended conformation and insert tryptophan residues into tandem hydrophobic pockets exposed at the surface of the NOT9 subunit (also known as CAF40) of the CCR4–NOT complex and probably into additional pockets in NOT1 that remain to be identified (Chen *et al*, 2014; Mathys *et al*, 2014).

Similar to GW182 proteins, the Nanos NBR not only contacts NOT1 but also binds to NOT3, providing the first detailed insight into how an mRNA-binding protein recruits the CCR4–NOT complex by contacting two of its subunits simultaneously. Interestingly, the surface on NOT1 that is contacted by *Dm* Nanos partially overlaps with the binding surface for NOT4 as observed in the *Saccharomyces cerevisiae* (*Sc*) complex (Bhaskar *et al*, 2015). This would suggest that *Dm* Nanos competes with NOT4 for binding to NOT1, providing additional opportunities for the regulation of gene expression. However, it is not known whether the NOT4 binding mode is conserved between *Dm* and *Sc* because NOT4 does not co-purify with the CCR4–NOT complex in metazoans (Lau *et al*, 2009; Temme *et al*, 2010) and the *Sc* NOT4 sequences that bind NOT1 are not well conserved in metazoans (Bhaskar *et al*, 2015).

Together with previous studies (Fabian *et al*, 2013; Bhandari *et al*, 2014; Chen *et al*, 2014; Mathys *et al*, 2014), our results reveal that the recruitment of the CCR4–NOT complex is mediated by highly diverse sequence motifs and distinct binding modes. We speculate that these motifs represent a combinatorial code that is read by the CCR4–NOT complex to funnel the effects of diverse RNA-binding proteins into a common repressive pathway, which results in the removal of the mRNA poly(A) tail, translational repression, and, depending on the cellular context, full degradation of the mRNA.

Materials and Methods

DNA constructs

The DNA constructs used in this study are provided in the Appendix Supplementary Materials and Methods and are listed in Appendix Table S1. All of the constructs and mutations were confirmed by sequencing.

Tethering assays and dsRNA interference

For the λN-tethering assay, 2.5×10^6 S2 cells were seeded in 6-well plates and co-transfected with the following plasmids: 0.1 μg of reporter plasmid (F-Luc-5BoxB, F-Luc-5BoxB-$A_{95}C_7$-HhR or F-Luc), 0.4 μg of R-Luc-A_{90}-HhR, and 25 ng of plasmid expressing λN-HA or 2.5–25 ng of plasmid expressing λN-HA–Nanos protein fusions. For the assay using F-Luc-*hb*, cells were co-transfected with the following plasmids: 0.2 μg of F-Luc-*hb* reporter plasmid, 0.4 μg of R-Luc-A_{90}-HhR, and 20–30 ng of plasmids expressing GFP-Nanos fusion proteins. Cells were harvested 3 days after transfection.

Knockdowns using dsRNA were performed as previously described (Behm-Ansmant *et al*, 2006). To measure the mRNA half-life, cells were treated with actinomycin D (5 μg/ml final concentration) three days post-transfection and collected at the indicated time points. Firefly and Renilla luciferase activities were

measured using a Dual-Luciferase Reporter Assay system (Promega). Northern blotting was performed as previously described (Behm-Ansmant *et al*, 2006).

Tethering assays in human cells using the β-globin reporter containing six MS2 binding sites (6xbs; Lykke-Andersen *et al*, 2000) were performed as previously described (Bhandari *et al*, 2014). The transfection mixtures contained 0.1 or 1 μg of plasmids expressing MS2-HA-tagged Nanos or the NED fragment, respectively.

Co-immunoprecipitation assays and Western blotting

For co-immunoprecipitation assays in S2 cells, 2.5×10^6 cells were seeded per well in 6-well plates and transfected using Effectene transfection reagent (Qiagen). The transfection mixtures contained 1 μg of plasmid expressing HA-tagged deadenylase or decapping factors and 1–2 μg of GFP-tagged Nanos (either full length or fragments). Cells were harvested 3 days after transfection, and co-immunoprecipitation assays were performed as previously described (Braun *et al*, 2011). Co-immunoprecipitation assays in human cells were performed as previously described (Bhandari *et al*, 2014). All Western blots were developed with the ECL Western Blotting Detection System (GE Healthcare) according to the manufacturer's recommendations. Antibodies used in this study are listed in Appendix Table S2.

Protein expression and purification

All proteins for crystallization and *in vitro* pull-down assays were expressed in *E. coli* BL21 (DE3) Star cells (Invitrogen) in ZY medium at 20°C overnight. A detailed description of the purification procedures is included in the Appendix Supplementary Materials and Methods.

Crystallization, data collection, and structure determination

A detailed description of the crystallization conditions and the structure determination process is included in the Appendix Supplementary Materials and Methods. All diffraction data sets were recorded on a PILATUS 6M detector at the PXII beamline of the Swiss Light Source at a temperature of 100 K. The diffraction data and refinement statistics are summarized in Table 1.

In vitro GST pull-down assays

In vitro pull-down assays were performed as previously described (Bhandari *et al*, 2014). Briefly, purified GST-tagged Nanos (full length or fragments) was incubated with untagged NOT module and Protino glutathione agarose 4B beads (Macherey-Nagel) in pull-down buffer containing 50 mM HEPES (pH 7.5), 200 mM NaCl, and 2 mM DTT. After a 1 h incubation, the beads were washed four times with pull-down buffer. The proteins were eluted using pull-down buffer supplemented with 25 mM glutathione, precipitated with trichloroacetic acid, and analyzed by SDS–PAGE.

For the experiment shown in Fig 7C, 25×10^6 S2 cells were suspended in 1 ml of hypotonic buffer (10 mM HEPES (pH 7.6), 1.5 mM $MgCl_2$, 10 mM KCl, 1 mM DTT, and 1× Roche-EDTA free protease inhibitor cocktail) for 15 min on ice. Cells were lysed by sonication (3 times for 30 s followed by 30 s on ice) followed by applying 10 strokes of a Dounce homogenizer. Cell lysates were supplemented with 200 mM NaCl. Cell debris was removed by 15-min centrifugation at 16,000 × *g* at 4°C. The supernatant was collected, treated with RNase A, and supplemented with 40 μg of purified GST-tagged Nanos NBR peptide (wild type or mutant) and 40 μl Protino glutathione agarose 4B beads (Macherey-Nagel). After 1.5 h incubation on a rotating wheel at 4°C, the beads were washed three times with binding buffer (hypotonic buffer supplemented with 200 mM NaCl). Bound proteins were eluted in 50 μl of binding buffer containing 25 mM reduced glutathione solution and analyzed by SDS–PAGE and Western blotting.

Accession numbers

The structures were deposited in the Protein Data Bank under accession codes 5FU6 for the NOT module and 5FU7 for the NOT module with the NBR peptide.

Expanded View for this article is available online.

Acknowledgements
We are grateful to Heike Budde and Catrin Weiler for excellent technical support. We thank the staff at the PX beamlines of the Swiss Light Source, Villigen, for assistance with data collection. This work was supported by the Max Planck Society and the Gottfried Wilhelm Leibniz Program awarded to E.I.

Author contributions
TR and KS cloned, expressed, and purified proteins for crystallization and pull-down assays. TR and KS crystallized the NOT module mutant and the NOT module–Nanos complex. TR solved the structures and performed *in vitro* pull-down assays. DB and SH cloned proteins for expression in human and S2 cells. SH carried out co-immunoprecipitation assays. DB designed, performed, and analyzed functional assays in human and S2 cells. EV and OW supervised the structural studies and assisted with refinement. EV designed the NOT module crystallization mutant. OW conceived and analyzed the selenomethionine experiment. EI designed and supervised the project. EI and OW wrote the manuscript with help from TR, DB, and EV.

Conflict of interest
The authors declare that they have no conflict of interest.

References

Arrizabalaga G, Lehmann R (1999) A selective screen reveals discrete functional domains in *Drosophila* Nanos. *Genetics* 153: 1825 – 1838

Asaoka-Taguchi M, Yamada M, Nakamura A, Hanyu K, Kobayashi S (1999) Maternal Pumilio acts together with Nanos in germline development in *Drosophila* embryos. *Nat Cell Biol* 1: 431 – 437

Baines RA (2005) Neuronal homeostasis through translational control. *Mol Neurobiol* 32: 113 – 121

Barckmann B, Simonelig M (2013) Control of maternal mRNA stability in germ cells and early embryos. *Biochim Biophys Acta* 1829: 714 – 724

Bawankar P, Loh B, Wohlbold L, Schmidt S, Izaurralde E (2013) NOT10 and C2orf29/NOT11 form a conserved module of the CCR4-NOT complex that docks onto the NOT1 N-terminal domain. *RNA Biol* 10: 228 – 244

Behm-Ansmant I, Rehwinkel J, Doerks T, Stark A, Bork P, Izaurralde E (2006) mRNA degradation by miRNAs and GW182 requires both CCR4:NOT deadenylase and DCP1:DCP2 decapping complexes. *Genes Dev* 20: 1885 – 1898

Bhandari D, Raisch T, Weichenrieder O, Jonas S, Izaurralde E (2014) Structural basis for the Nanos-mediated recruitment of the CCR4-NOT complex and translational repression. *Genes Dev* 28: 888 – 901

Bhaskar V, Basquin J, Conti E (2015) Architecture of the ubiquitylation module of the yeast Ccr4-Not complex. *Structure* 23: 921 – 928

Bhaskar V, Roudko V, Basquin J, Sharma K, Urlaub H, Seraphin B, Conti E (2013) Structure and RNA-binding properties of the Not1-Not2-Not5 module of the yeast Ccr4-Not complex. *Nat Struct Mol Biol* 20: 1281 – 1288

Boland A, Chen Y, Raisch T, Jonas S, Kuzuoğlu-Öztürk D, Wohlbold L, Weichenrieder O, Izaurralde E (2013) Structure and assembly of the NOT module of the human CCR4-NOT complex. *Nat Struct Mol Biol* 20: 1289 – 1297

Braun JE, Huntzinger E, Fauser M, Izaurralde E (2011) GW182 proteins directly recruit cytoplasmic deadenylase complexes to miRNA targets. *Mol Cell* 44: 120 – 133

Chagnovich D, Lehmann R (2001) Poly(A)-independent regulation of maternal *hunchback* translation in the *Drosophila* embryo. *Proc Natl Acad Sci USA* 98: 11359 – 11364

Chekulaeva M, Mathys H, Zipprich JT, Attig J, Colic M, Parker R, Filipowicz W (2011) miRNA repression involves GW182-mediated recruitment of CCR4-NOT through conserved W-containing motifs. *Nat Struct Mol Biol* 18: 1218 – 1226

Chen Y, Boland A, Kuzuoğlu-Öztürk D, Bawankar P, Loh B, Chang CT, Weichenrieder O, Izaurralde E (2014) A DDX6-CNOT1 complex and W-binding pockets in CNOT9 reveal direct links between miRNA target recognition and silencing. *Mol Cell* 54: 737 – 750

Chicoine J, Benoit P, Gamberi C, Paliouras M, Simonelig M, Lasko P (2007) Bicaudal-C recruits CCR4-NOT deadenylase to target mRNAs and regulates oogenesis, cytoskeletal organization, and its own expression. *Dev Cell* 13: 691 – 704

Cooke A, Prigge A, Wickens M (2010) Translational repression by deadenylases. *J Biol Chem* 285: 28506 – 28513

Curtis D, Treiber DK, Tao F, Zamore PD, Williamson JR, Lehmann R (1997) A CCHC metal-binding domain in Nanos is essential for translational regulation. *EMBO J* 16: 834 – 843

Davey NE, Van Roey K, Weatheritt RJ, Toedt G, Uyar B, Altenberg B, Budd A, Diella F, Dinkel H, Gibson TJ (2012) Attributes of short linear motifs. *Mol BioSyst* 8: 268 – 281

Fabian MR, Frank F, Rouya C, Siddiqui N, Lai WS, Karetnikov A, Blackshear PJ, Nagar B, Sonenberg N (2013) Structural basis for the recruitment of the human CCR4-NOT deadenylase complex by tristetraprolin. *Nat Struct Mol Biol* 20: 735 – 739

Ginter-Matuszewska B, Kusz K, Spik A, Grzeszkowiak D, Rembiszewska A, Kupryjanczyk J, Jaruzelska J (2011) NANOS1 and PUMILIO2 bind microRNA biogenesis factor GEMIN3, within chromatoid body in human germ cells. *Histochem Cell Biol* 136: 279 – 287

Goldstrohm AC, Hook BA, Seay DJ, Wickens M (2006) PUF proteins bind Pop2p to regulate messenger RNAs. *Nat Struct Mol Biol* 13: 533 – 539

Gupta YK, Lee TH, Edwards TA, Escalante CR, Kadyrova LY, Wharton RP, Aggarwal AK (2009) Co-occupancy of two Pumilio molecules on a single *hunchback* NRE. *RNA* 15: 1029 – 1035

Hashimoto H, Hara K, Hishiki A, Kawaguchi S, Shichijo N, Nakamura K, Unzai S, Tamaru Y, Shimizu T, Sato M (2010) Crystal structure of zinc-finger domain of Nanos and its functional implications. *EMBO Rep* 11: 848 – 853

Igreja C, Izaurralde E (2011) CUP promotes deadenylation and inhibits decapping of mRNA targets. *Genes Dev* 25: 1955 – 1967

Jaruzelska J, Kotecki M, Kusz K, Spik A, Firpo M, Reijo Pera RA (2003) Conservation of a Pumilio-Nanos complex from *Drosophila* germ plasm to human germ cells. *Dev Genes Evol* 213: 120 – 126

Joly W, Chartier A, Rojas-Rios P, Busseau I, Simonelig M (2013) The CCR4 Deadenylase Acts with Nanos and Pumilio in the Fine-Tuning of Mei-P26 Expression to Promote Germline Stem Cell Self-Renewal. *Stem Cell Reports* 1: 411 – 424

Kadyrova LY, Habara Y, Lee TH, Wharton RP (2007) Translational control of maternal Cyclin B mRNA by Nanos in the *Drosophila* germline. *Development* 134: 1519 – 1527

Kyte J, Doolittle RF (1982) A simple method for displaying the hydropathic character of a protein. *J Mol Biol* 157: 105 – 132

Lai F, King ML (2013) Repressive translational control in germ cells. *Mol Reprod Dev* 80: 665 – 676

Lai F, Zhou Y, Luo X, Fox J, King ML (2011) Nanos1 functions as a translational repressor in the Xenopus germline. *Mech Dev* 128: 153 – 163

Lau NC, Kolkman A, van Schaik FM, Mulder KW, Pijnappel WW, Heck AJ, Timmers HT (2009) Human Ccr4-Not complexes contain variable deadenylase subunits. *Biochem J* 422: 443 – 453

Lehmann R, Nüsslein-Volhard C (1991) The maternal gene *nanos* has a central role in posterior pattern formation of the *Drosophila* embryo. *Development* 112: 679 – 691

Leppek K, Schott J, Reitter S, Poetz F, Hammond MC, Stoecklin G (2013) Roquin promotes constitutive mRNA decay via a conserved class of stem-loop recognition motifs. *Cell* 153: 869 – 881

Loedige I, Jakob L, Treiber T, Ray D, Stotz M, Treiber N, Hennig J, Cook KB, Morris Q, Hughes TR, Engelmann JC, Krahn MP, Meister G (2015) The Crystal Structure of the NHL Domain in Complex with RNA Reveals the Molecular Basis of *Drosophila* Brain-Tumor-Mediated Gene Regulation. *Cell Rep* 13: 1206 – 1220

Loedige I, Stotz M, Qamar S, Kramer K, Hennig J, Schubert T, Löffler P, Längst G, Merkl R, Urlaub H, Meister G (2014) The NHL domain of BRAT is an RNA-binding domain that directly contacts the *hunchback* mRNA for regulation. *Genes Dev* 28: 749 – 764

Lykke-Andersen J, Shu MD, Steitz JA (2000) Human Upf proteins target an mRNA for nonsense-mediated decay when bound downstream of a termination codon. *Cell* 103: 1121 – 1131

Mathys H, Basquin J, Ozgur S, Czarnocki-Cieciura M, Bonneau F, Aartse A, Dziembowski A, Nowotny M, Conti E, Filipowicz W (2014) Structural and Biochemical Insights to the Role of the CCR4-NOT Complex and DDX6 ATPase in MicroRNA Repression. *Mol Cell* 54: 751 – 765

Miles WO, Tschop K, Herr A, Ji JY, Dyson NJ (2012) Pumilio facilitates miRNA regulation of the E2F3 oncogene. *Genes Dev* 26: 356 – 368

Mochizuki K, Sano H, Kobayashi S, Nishimiya-Fujisawa C, Fujisawa T (2000) Expression and evolutionary conservation of nanos-related genes in Hydra. *Dev Genes Evol* 210: 591 – 602

Murata Y, Wharton RP (1995) Binding of pumilio to maternal *hunchback* mRNA is required for posterior patterning in *Drosophila* embryos. *Cell* 80: 747 – 756

Semotok JL, Cooperstock RL, Pinder BD, Vari HK, Lipshitz HD, Smibert CA (2005) Smaug recruits the CCR4/POP2/NOT deadenylase complex to trigger maternal transcript localization in the early *Drosophila* embryo. *Current Biol* 15: 284 – 294

Sonoda J, Wharton RP (1999) Recruitment of Nanos to *hunchback* mRNA by Pumilio. *Genes Dev* 13: 2704 – 2712

Sonoda J, Wharton RP (2001) *Drosophila* Brain Tumor is a translational repressor. *Genes Dev* 15: 762 – 773

Subramaniam K, Seydoux G (1999) *nos-1* and *nos-2*, two genes related to *Drosophila nanos*, regulate primordial germ cell development and survival in *Caenorhabditis elegans*. *Development* 126: 4861 – 4871

Suzuki A, Igarashi K, Aisaki K, Kanno J, Saga Y (2010) NANOS2 interacts with the CCR4-NOT deadenylation complex and leads to suppression of specific RNAs. *Proc Natl Acad Sci USA* 107: 3594 – 3599

Suzuki A, Saba R, Miyoshi K, Morita Y, Saga Y (2012) Interaction between NANOS2 and the CCR4-NOT deadenylation complex is essential for male germ cell development in mouse. *PLoS ONE* 7: e33558

Temme C, Simonelig M, Wahle E (2014) Deadenylation of mRNA by the CCR4-NOT complex in *Drosophila*: molecular and developmental aspects. *Front Genet* 5: 143

Temme C, Zhang L, Kremmer E, Ihling C, Chartier A, Sinz A, Simonelig M, Wahle E (2010) Subunits of the *Drosophila* CCR4-NOT complex and their roles in mRNA deadenylation. *RNA* 16: 1356 – 1370

Tsuda M, Sasaoka Y, Kiso M, Abe K, Haraguchi S, Kobayashi S, Saga Y (2003) Conserved role of nanos proteins in germ cell development. *Science* 301: 1239 – 1241

Van Etten J, Schagat TL, Hrit J, Weidmann C, Brumbaugh J, Coon JJ, Goldstrohm AC (2012) Human Pumilio proteins recruit multiple deadenylases to efficiently repress messenger RNAs. *J Biol Chem* 287: 36370 – 36383

Verrotti AC, Wharton RP (2000) Nanos interacts with cup in the female germline of *Drosophila*. *Development* 127: 5225 – 5232

Wang C, Lehmann R (1991) Nanos is the localized posterior determinant in *Drosophila*. *Cell* 66: 637 – 647

Wang X, McLachlan J, Zamore PD, Hall TM (2002) Modular recognition of RNA by a human pumilio-homology domain. *Cell* 110: 501 – 512

Weidmann CA, Goldstrohm AC (2012) *Drosophila* Pumilio protein contains multiple autonomous repression domains that regulate mRNAs independently of Nanos and brain tumor. *Mol Cell Biol* 32: 527 – 540

Wharton RP, Sonoda J, Lee T, Patterson M, Murata Y (1998) The Pumilio RNA-binding domain is also a translational regulator. *Mol Cell* 1: 863 – 872

Wharton RP, Struhl G (1991) RNA regulatory elements mediate control of *Drosophila* body pattern by the posterior morphogen nanos. *Cell* 67: 955 – 967

Wreden C, Verrotti AC, Schisa JA, Lieberfarb ME, Strickland S (1997) Nanos and pumilio establish embryonic polarity in *Drosophila* by promoting posterior deadenylation of *hunchback* mRNA. *Development* 124: 3015 – 3023

Zamore PD, Williamson JR, Lehmann R (1997) The Pumilio protein binds RNA through a conserved domain that defines a new class of RNA-binding proteins. *RNA* 3: 1421 – 1433

Zekri L, Kuzuoğlu-Öztürk D, Izaurralde E (2013) GW182 proteins cause PABP dissociation from silenced miRNA targets in the absence of deadenylation. *EMBO J* 32: 1052 – 1065

